Journal of Rehabilitation in Civil Engineering 10-4 (2022) 129-145

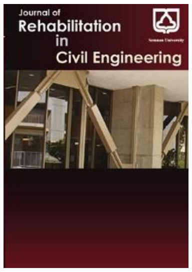


journal homepage: http://civiljournal.semnan.ac.ir/

# Multi-Objective Aerodynamic Optimization of the Exterior Shape of Tall Buildings with Trilateral Cross-Section

**M. Noormohamadian[1*], E. Salajegheh[2]**

1. Ph.D Student, Department of Civil Engineering, Shahid Bahonar University of Kerman, Iran
2. Professor, Department of Civil Engineering, Shahid Bahonar University of Kerman, Iran
Corresponding author: mehdi.noormohamadian@gmail.com

**ARTICLE INFO**

Article history:
Received: 06 June 2021
Revised: 19 December 2021
Accepted: 20 December 2021

Keywords:
Aerodynamic Modifications;
Wind Load;
Tall Building;
Computational Fluid Dynamic;
Multi-Objective Optimization;
Artificial Neural Networks.

## ABSTRACT

Wind-induced loads are largely dependent upon the exterior shape of buildings, and one highly effective procedure to mitigate them is to apply aerodynamic shape modifications in the aerodynamic optimization procedure (AOP). This study presents the framework of an AOP for shape modifications of the trilateral cross-section tall buildings. The AOP is comprised of a combination of multi-objective optimization algorithm named non-dominated sorting genetic algorithm II (NSGA-II), artificial neural networks, and computational fluid dynamics. The building shape is designed based on the geometric description of its vertical and horizontal profile using seven geometric parameters (design variables) to apply different types and sizes of modifications. In addition, the mean moment coefficients in drag and lift directions are considered as the objective functions. The proposed procedure investigates the effect of the three types of modifications including varying cross-section sizes along the height, twisting, and curved-side on the reduction of objective functions. Finally, a set of optimal building shapes is presented as the Pareto front solutions, which enables the designers to select the optimal shape of the building with additional considerations. The results indicate the high capability of the proposed framework to make appropriate use of various aerodynamic modifications in order to upgrade the aerodynamic performance of the trilateral cross-section tall buildings.

**How to cite this article:**
Noormohamadian, M., Salajegheh, E. (2022). Multi-objective aerodynamic optimization of the exterior shape of tall buildings with trilateral cross-section. Journal of Rehabilitation in Civil Engineering, 10(4), 129-145.
https://doi.org/10.22075/JRCE.2021.23611.1515

## 1. Introduction

Nowadays, rising demand for tall buildings is due to population growth, scarcity, and extravagant land expenses. Wind load is customarily considered as the dominant lateral load in tall building design. Thus, examining the effect of wind load on tall buildings and exploring the effective solutions to minimize its influence have been the subject of much research. Wind load can be controlled by the exterior shape modification that can alter the pattern of wind flow surrounding the buildings, and provide the designers with the possibility to reduce the aerodynamic response of the building in along-wind and across-wind directions with exterior shape modifications in such a way to lessen construction costs.

The along-wind load results from pressure fluctuations in windward and leeward faces. The along-wind responses can be reduced significantly by the corner modifications such as slotted corners, corner recession, chamfered corners, curved side and roundness, which are normally classified as minor aerodynamic modifications. A wide range of research has been performed on minor aerodynamic modifications at different cross-sections and the effect of the modifications on reducing along-wind responses [1]–[7]. Twisting, tapering, opening, setback, varying cross-section size, and shape can reduce significantly across-wind response as major modifications [8]–[17]. Tamura et al. [18], [19] conducted comprehensive research on the aerodynamic modifications for different building shapes in the form of square, circle, triangular, rectangular, and ellipsoidal cross sections. Additionally, the effects of minor and major modifications including corner cut, corner chamfered, setback, twist, and tapered on the aerodynamic responses were investigated. The results provide designers with comprehensive and applicable data on the initial design of the building. In these studies, different types of modifications based on a single set of sizes for each modification have been compared and the effect of each is examined to reduce the aerodynamic responses, separately.

The effectiveness of aerodynamic modifications can be enhanced using an aerodynamic optimization procedure (AOP) which determines the optimal combination of modifications based on an investigation of various types and sizes of modification in a wide search space [20]. It means that in AOP, a wide range of different modifications can be explored by selecting the appropriate design variables. Kareem et al. [20] presented an optimization framework for corner modification of rectangular cross-section buildings. In this framework, corner shape modification was investigated based on seven control points as design variables. Bernardini et al. [21] used positions of two control points (design variables) to determine the shape of a spline curve as the corner shape of a square cross-section. The objective function can be estimated at each iteration process of AOP through computational fluid dynamic (CFD) analysis. Since this analysis entails a high computational expense, it is essential to use the surrogate model. In the research performed by Bernardini et al [21] the Kriging model was used as a surrogate model to evaluate the drag and lift coefficients (objective functions). Elshaer et al. [22] obtained the optimal corner shape of a square cross-section based on two design variables, and investigated the various types of corner modifications. Elshaer and Bitsuamlak [23] applied the artificial neural network (ANN) model as the surrogate model to evaluate the objective function at each iteration process and corroborated that the surrogate model can contribute to acceptable saving in calculation time. The findings revealed that the ANN model properly fitted the training database, and obtained a correlation coefficient of 0.979, resulting in an effective ANN model to estimate the aerodynamic responses of the building.

The present article aimed to investigate the effects of the exterior shape of the trilateral cross section tall buildings on the aerodynamic response in the AOP. For validation, the velocity and turbulence intensity profiles from the basic triangular model in the present research were compared to the experimental findings presented in [3], which have similar boundary conditions [24]. The exterior shape of the building was generated by seven geometric parameters, are as the design variables that described in Section 3, which can produce a wide search space with various types and size of modifications. The mean moment coefficients in drag and lift directions as objective functions were used to compare the aerodynamic performance of different models. These functions were optimized in a two-objective optimization process using the non-dominated sorting genetic algorithm II (NSGAII). To evaluate the objective functions, the ANN model was used as a surrogate model instead of CFD analysis. Ultimately, an optimal combination of modifications was obtained in the present research.

## 2. Aerodynamic optimization procedure (AOP)

The first step in AOP is defining design variables and objective functions. Appropriate design variables can create a wide range of shape modifications. It should be noted that to satisfy the structural and architectural requirements for acceptable shapes, a set of constraints on design variables should be considered. Then, mean moment coefficients in drag and lift directions as the objective functions were evaluated to a set of random combinations of geometry parameters in various wind angles of attack (AOAs) using the CFD method. The generated database was used to train the ANN model, and the model evaluates objective functions. Fig. 1 shows the framework used for the aerodynamic optimization procedure (AOP).

## 3. Geometric modeling of exterior shape of building

Horizontal and vertical profiles of the building can be described by building shape parameters. These parameters are design variables of the optimization process that generate aerodynamic modifications on the building. The horizontal and vertical profiles are defined by quadratic and cubic functions, respectively.

### 3.1. Geometry description of vertical profile

The vertical profile of the building is defined by a cubic function according to Eq. 1. Here, a0, a1, a2, and a3 are coefficients of the cubic function. This function can apply the modification of the cross-section variations along the building height. Where bzi (Eq. 2) represents the y at corresponding height, zi. An example of the vertical profile of a building is demonstrated in Fig. 2.

$$y(z) = a_0 + a_1 z + a_2 z^2 + a_3 z^3 \quad (1)$$

$$b_{zi} = a_0 + a_1 z_i + a_2 z_i^2 + a_3 z_i^3 \quad (2)$$

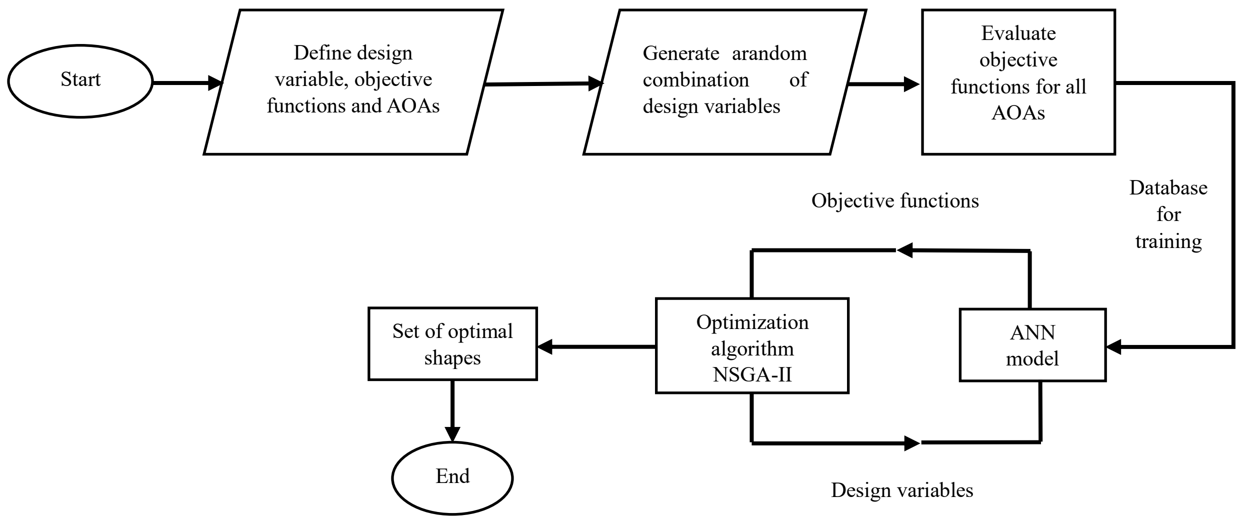


**Fig. 1.** The framework of Aerodynamic Optimization Procedure (AOP).

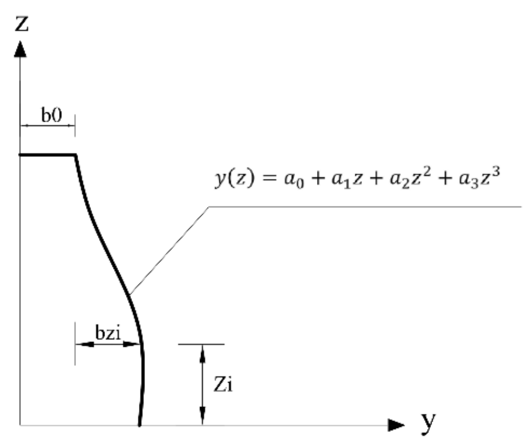


**Fig. 2.** Vertical profile geometry.

## 3.2. Geometry description of the horizontal profile

The curved sides of the trilateral models are determined by a quadratic function using Eq. 3, where b0 and b1 are coefficients of a quadratic function. Fig. 3 shows a basic triangular cross-section with vertices A, B, and C. The circle with radius of R passes through the three vertices of the basic equilateral triangle (A, B and C) to define the range of geometric variations. On the other hand, the triangle with curved sides shown in Fig.3 displays the cross-section of the modified building. The cross-section modeling consists of two stages:

1. Find the curve passes through points A and B based on Eq. 3. The coordinates of the points were obtained from Eqs. 4 and 5.

2. The AC and BC are obtained through mirroring AB relative to OB and OC lines, respectively, and the closed form of the cross section is achieved.

$$y(x) = b_0 + b_1 x^2 + b_z \tag{3}$$

$$x_A = Rcos(30°), \quad y_A = Rsin(30°) \tag{4}$$

$$x_B = -Rcos(30°), \quad y_B = Rsin(30°) \tag{5}$$

Coefficient b1 represents the degree of curvature of the cross-section. The triangle cross-section is obtained when b1 = 0. Here,

$b_{zi}$ that is calculated from Eq. 2 indicates the cross-section size variations along the z-axis.

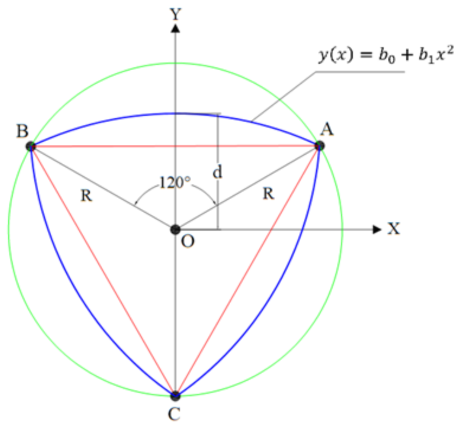


**Fig. 3**. Horizontal profile geometry.

Another geometry parameter that plays an important part in reducing wind-induced loads is the twist, T, which is taken as the seventh design variable in modeling. Therefore, geometric parameters ($a_0$, $a_1$, $a_2$, $a_3$, $b_0$, $b_1$ and T) are design variables in the optimization problem. The effects of the three types of modifications including varying cross-section sizes along the height, twisting, and curved-side on the exterior shape of the building are evaluated based on the geometric parameters, and represented in Fig. 4.

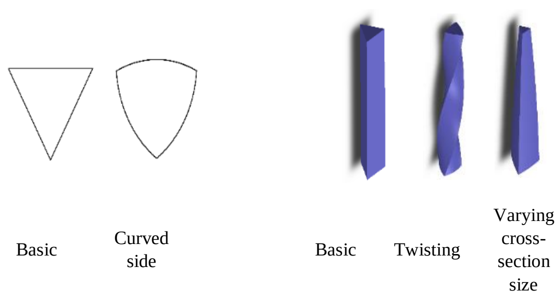


**Fig. 4**. Types of modifications applied to the exterior forming process.

## 4. CFD analysis

To produce a database for training the ANN model, a set of design variables, angle of attack (AOA), and corresponding objective function are required and can be provided with CFD analysis. Four AOAs (0°, 30°, 60°, & 90°) for each model are considered, and presented in Fig. 5. Therefore, given the symmetry of the cross-section, 12 states of AOAs with $30^0$ interval were investigated.

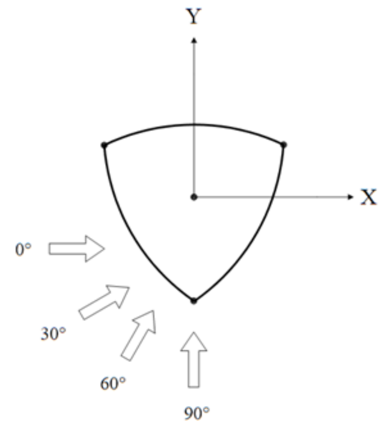


**Fig. 5**. The wind direction on the building.

Using Solidworks 2015 software [25], an initial graphics specification (IGES) file was created for each of the samples, which was readable by the CFD solver. Fluent 17.1 [26] was utilized to solve the CFD analysis, and mean moment coefficients in drag and lift directions were considered as the aerodynamic responses based on Eqs. 6 and 7.

$$C_{MD} = \frac{M_D}{q_H BH^2} \tag{6}$$

$$C_{ML} = \frac{M_L}{q_H BH^2} \tag{7}$$

Here, $M_D$ and $M_L$ are the base moments in the along-wind and across-wind directions, respectively, and $q_H$ is the velocity pressure at the height of model (H), and B is the width of the model.

For each sample by considering four AOAs, $C_{MD}$ and $C_{ML}$ values are calculated using the CFD method, and the critical wind direction response is chosen as the ultimate response of the model.

Since the main objective is to provide an approximate framework to estimate the effect of exterior shape modification on the aerodynamic responses, it is assumed that the building is a rigid body which acts as an obstacle to the airflow. Furthermore, the mean value of the responses was calculated by the steady-state method.

## 4.1. Boundary conditions

The vertical velocity profile U (z) is measured by Eq. 8, that proposed by the Working Group of the Architectural Institute of Japan (AIJ) [27].

$$U(z)=U_h\left(\frac{z}{z_h}\right)^{\alpha} \quad (8)$$

Where $U_h$ is the speed of wind at the top of the building, z is the building height, and α is an exponent of the velocity profile based on the building location which is assumed to be about 0.27 [18] for the building in the urban area. The wind velocity profile under the condition in which wind speed at the top of the building is 7 m/s is shown in Fig. 6(a).

The standard k-ε model as a model built upon Reynolds-Averaged Navier–Stokes (RANS) is widely applied in wind engineering due to its high efficiency and facile application, and its primary application is to predict the overall wind condition surrounding the building. However, modeling the flow separation zones adjacent to the side walls of the building and above roof surfaces [28] using the standard k- ε model leads to an extremely high estimation of turbulence energy in the windward corner zone. Thus, a modified k-ε model known as LK model was introduced by Launder and Kato [29] to improve the prediction of wind flow surrounding the buildings. In this study, the LK model that can yield rapid calculations and encouraging results is applied [30]. It is possible to estimate the vertical distribution of turbulent energy k(z) through a wind tunnel test or an observation of the surroundings. If it would not be feasible, k(z) can be also obtained by Eq. (9) on the basis of the estimation equation for the vertical profile of turbulent intensity I(z) proposed by Architectural Institute of Japan (AIJ) Recommendations (Eq. 10) and also by assuming $k(z) \cong \sigma_u^2(z) = (I(z)U(z))^2$ [27].

$$k(z)=\frac{\sigma_z^2(z)+\sigma_v^2(z)+\sigma_w^2(z)}{2} \quad (9)$$

Where σ represents the root mean square (RMS) velocity fluctuation.

$$I(z)=\frac{\sigma_u(z)}{U(z)}=0.1\left(\frac{z}{H}\right)^{(-\alpha-0.05)} \quad (10)$$

H is the building height, and $\sigma_u$ is the RMS velocity fluctuation along the stream-wise direction in the atmospheric boundary layer (ABL). The profile of the turbulent intensity is shown in Fig. 6 (b).

The vertical distribution of the kinetic energy k (z) is used to determine the dissipation rate, ε, at the inlet section by Eq. 11.

$$\varepsilon(z)=C_{\mu}^{0.5}k(z)\frac{U_h}{z_h}\alpha\left(\frac{z}{z_h}\right)^{(\alpha-1)} \quad (11)$$

Where $C_\mu$ is the constant of the model and equals to 0.09.

Fig. 7 illustrates other boundary conditions and computational domains when the computing domain is 1.8, 1.1, and 0.8 meters.

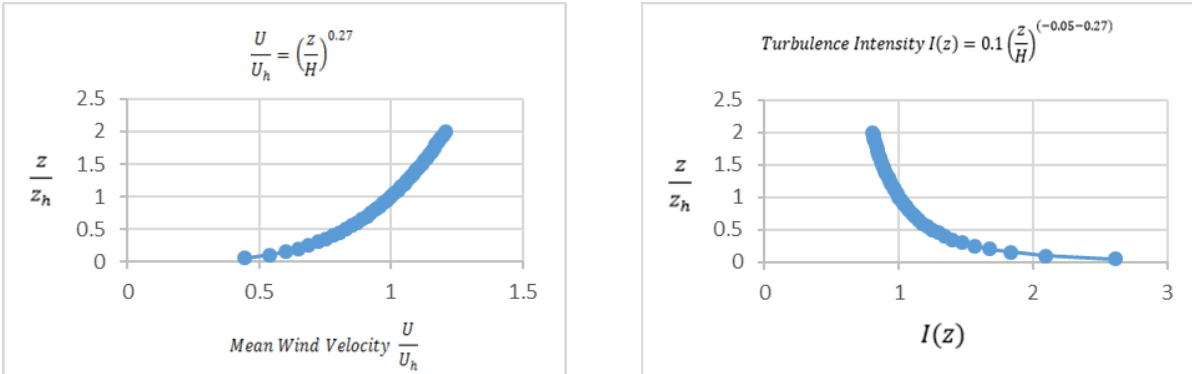


(a) (b)

**Fig. 6.** Inflow profiles: (a) Mean wind velocity profile and (b) Turbulence intensity profil.

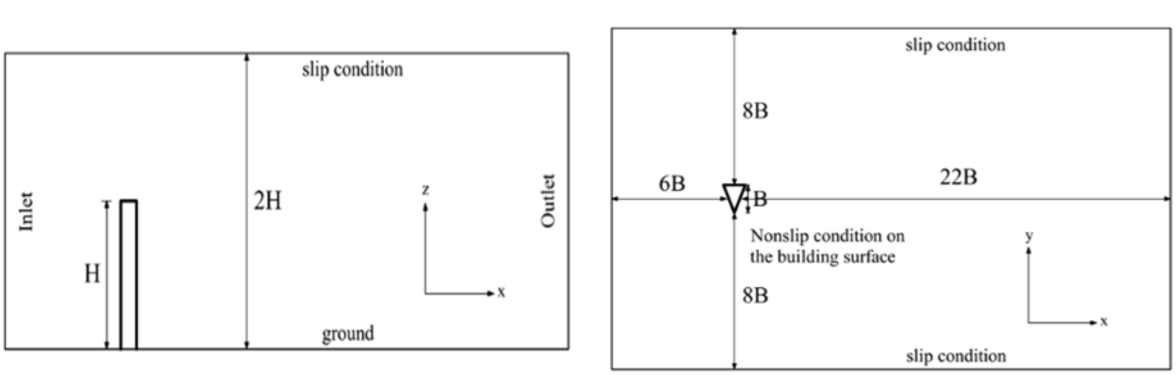


(a) (b)

**Fig. 6.** Computational domain and boundary conditions: (a) vertical plane, (b) horizontal plane in width, along the x, y, and z-axes respectively[31].

## 4.2. Mesh generation

To achieve a proper grid configuration, a comparison of the responses of the produced grids were made, and the largest mesh which was independent from the grids system was selected as the fine mesh. The turbulent flows on the surface were estimated using the dimensionless parameter of the wall, $y^+$. The parameter is calculated based on $y^+ = \left(\frac{\rho u y}{\mu}\right)$ in the fluent software and enables to select the appropriate grid configuration. Here, ρ is the density of air, u is the friction velocity of the air, μ is the kinematic viscosity of air, and y is the vertical distance normal to wall direction. In all grids, it is assumed that the velocity profile is laminar and viscous stress is governed by the wall shear, $y^+ < 5$. Thus, enhanced wall treatment can be used, and it is not required to define wall functions [26].

## 5. Optimization process

The commonly used methodology for multi-objective optimization problems is Non-dominated Sorting Genetic Algorithm II (NSGA-II) [32]–[34]. The multi-objective optimization problem involves two or more objective functions which have to be optimized concurrently, and there is not any unique solution that can optimize all objective functions. However, there is a set of Pareto optimal solutions called PF. All optimal solutions laying on the PF are considered equally appropriate. In NSGA-II, firstly, a parent population is randomly generated and the offspring population with size N is produced by using two operators namely crossover and mutation. Then, the sorting of the combined parent and offspring populations is conducted based on two criteria including non-domination rank and crowding distance. Indeed, the solutions with the lower ranks (lower non domination level) are preferred. In the case of the same ranks, the less crowded region is selected (higher crowding distance) [34]. N optimal solutions in this combined population is selected as the next parent population. This process is repeated until the solutions achieve convergence in successive generations. Finally, a PF is obtained that provides a set of optimal shapes with the appropriate aerodynamic performance among the entire search space. Therefore, the PF curve gives designers the opportunity to have further options to design the exterior shape of the building.

In addition, use of CFD method in each iteration process to evaluate objective functions is highly costly. To overcome this problem, researchers usually use some surrogate models, which ANN model is the surrogate model used in present study. The ANN model has widely been used in wind engineering [35]–[37]. The objective functions ($C_{ML}$ and $C_{MD}$) for each iteration are estimated by the ANN model, which significantly reduces computational time compared to CFD Analysis. The popular type of the artificial neural network (ANN) is the multilayer perceptron (MLP) that includes the input, hidden and output layers. Located between inputs and outputs, the hidden layers are applied to learn more complex features. Such layers sometimes are more than one layer [36], and carry out computations on the weighted inputs and then generate the output using the nonlinear activation function. Different activation functions can be studied in [38], [39].

MLP uses backpropagation for training the neural network as a supervised learning technique. Backpropagation is a repetitive process that adjusts weights in such a way to minimize the difference between target output and network prediction.

## 6. Numerical investigation

In this part, an example is presented to examine the proposed framework capability in upgrading the trilateral cross section aerodynamic performance. The example is provided with the following assumptions:

To generate the exterior shape of tall buildings, some constraints can be imposed in accordance with architectural and structural requirements. Therefore, Eqs. 12 to 14 were applied as constraints in the construction of building models. These constraints are taken into account differently based on the conditions of each project.

$$0.5R \le d \le 1.5R\,, \quad d = b_0 + b_z \tag{12}$$

$$b_1 \le 0, \qquad 0^{\circ} \le T \le 270^{\circ} \tag{13}$$

$$900{,}000m^3 \le V \le 1{,}100{,}000m^3 \tag{14}$$

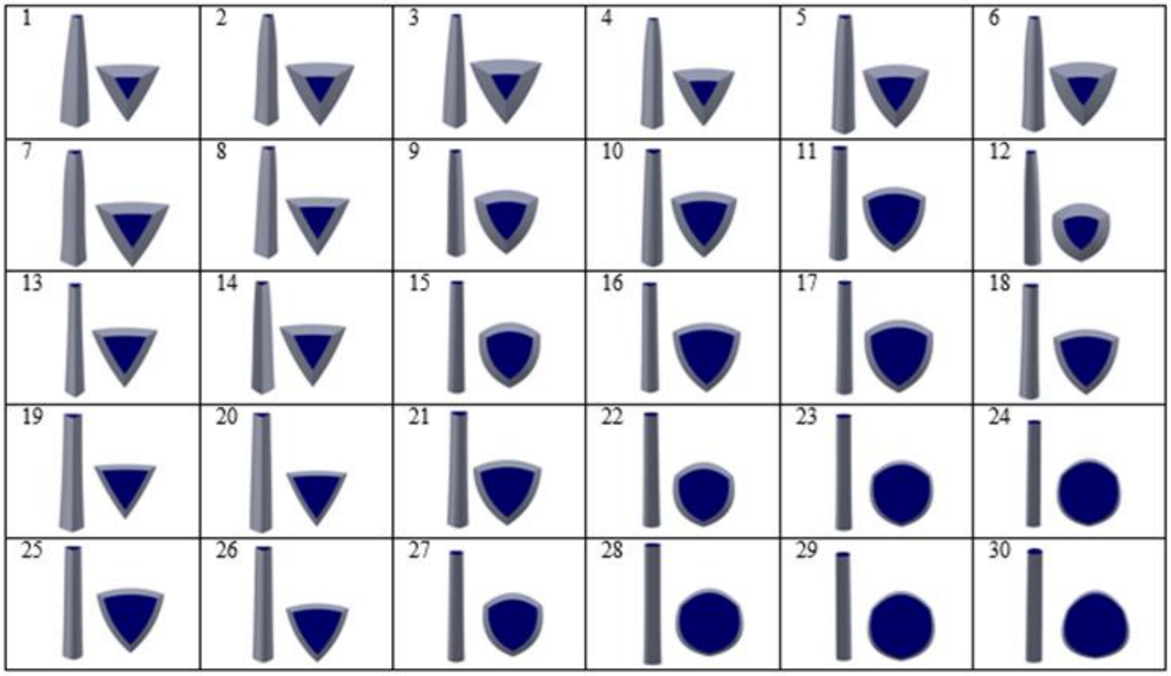


**Fig. 7.** Thirty different tall building geometries for an aerodynamic database generation.

Where d and R are the distance from curve to x-axis and radius of the circle, as shown in Fig 3. V denotes the volume of the building. Constraint $b_1<0$ means that in the optimization process, only the trilateral shapes whose sides have convex curvature are considered.

Based on the strategy applied to generate the exterior shape of the building provided in section 3, thirty models of building shapes were constructed using random combinations of the design variables ($a_0$, $a_1$, $a_2$, $a_3$, $b_0$ and $b_1$) (see Fig. 8). All models have a height of 400 meters with a scale of 1/1000. Four different twist angles based on Eq. 13, were applied for the models, and 120 samples produced for the purpose of ANN model training.

Different number of neurons was tested in MLP, and the hidden layer with 25 neurons brought about the optimal result. Furthermore, hyperbolic tangent sigmoid was used as activation function that gives a more accurate approximation of objective function than other activation functions. The schematic of MLP network shows in Fig. 9.

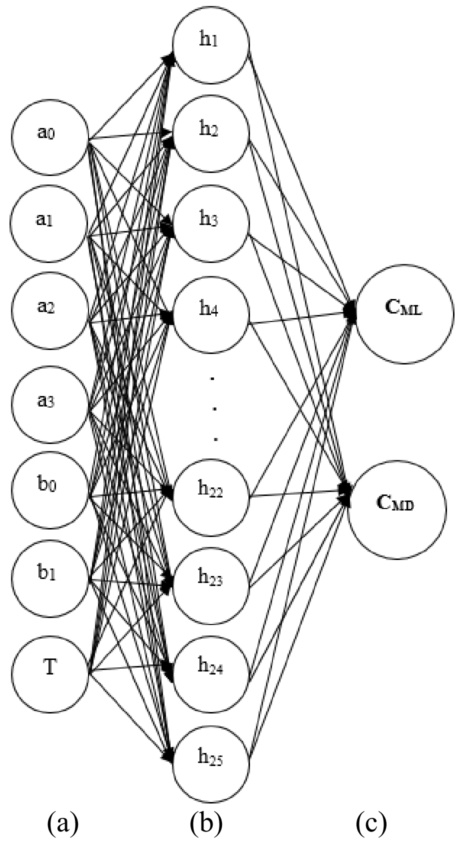


**Fig. 8.** Neural network model: (a) input layer, (b) hidden layer, and (c) output layer.

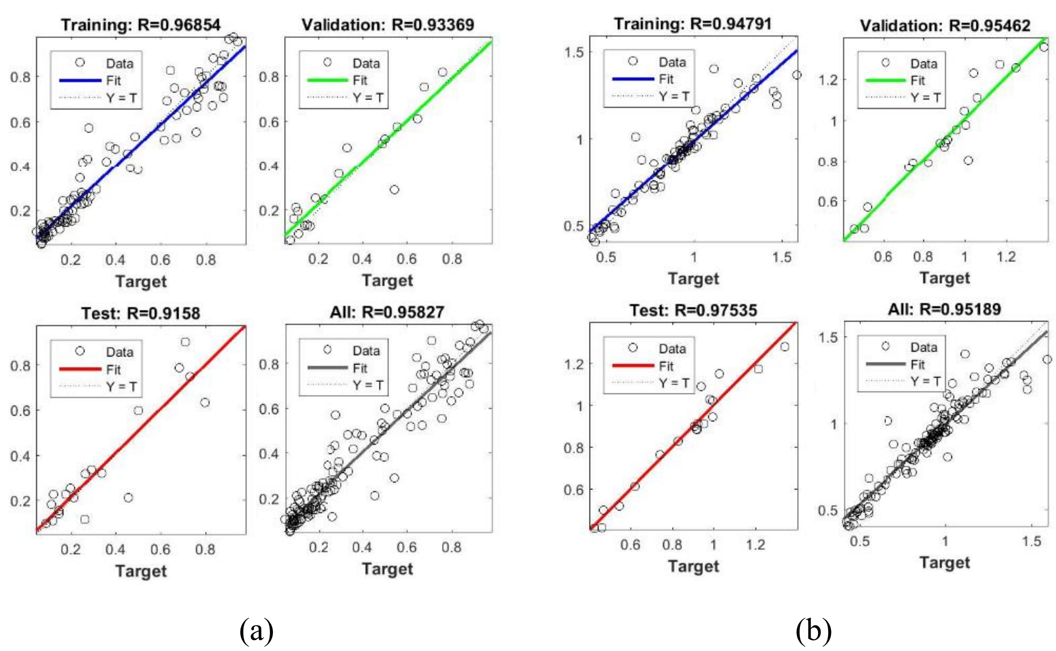


**Fig. 9.** Plot of ANN model regressions for approximating: (a) $C_{ML}$ and (b) $C_{MD.}$

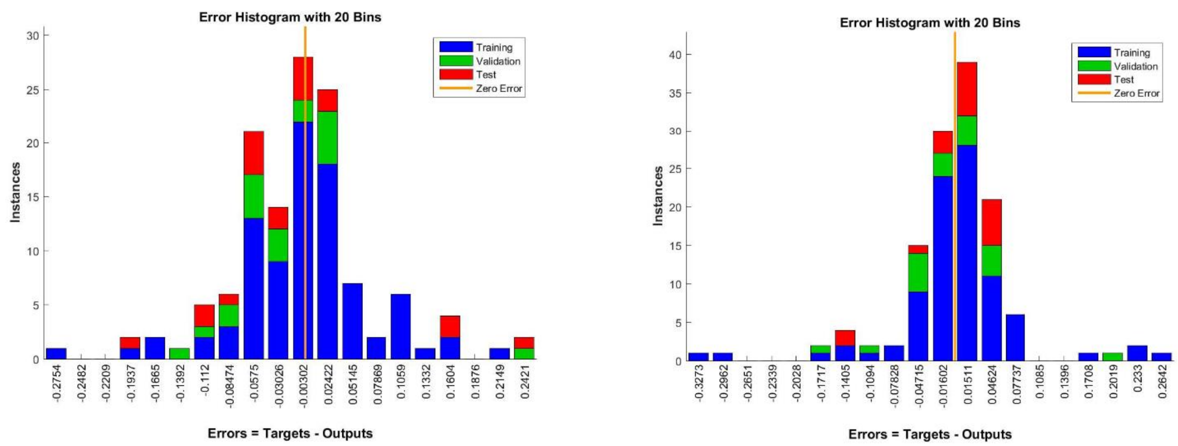


(a) (b)

**Fig. 10.** ANN model error distribution for: (a) $C_{ML}$ and (b) $C_{MD}$.

Input data for training, validation, and testing were assumed to be 70% (84 samples), 15% (18 samples), and 15% of total data, respectively. Fig. 10 shows the regression plot for the training, validation and testing samples. Furthermore, the correlation coefficients (R) relevant to the all data for $C_{ML}$ and $C_{MD,}$ are 0.96 and 0.95, respectively.

Fig. 11 presents the network error distributions, which explain the error of the ANN model in approximating the objective functions. In addition, according to the figure, the error in estimating for $C_{ML}$ is less than 6% in 80% of the all samples, and for $C_{MD}$ is 5% in 90% of the all samples. The results indicate adequate accuracy in approximating the objective functions.

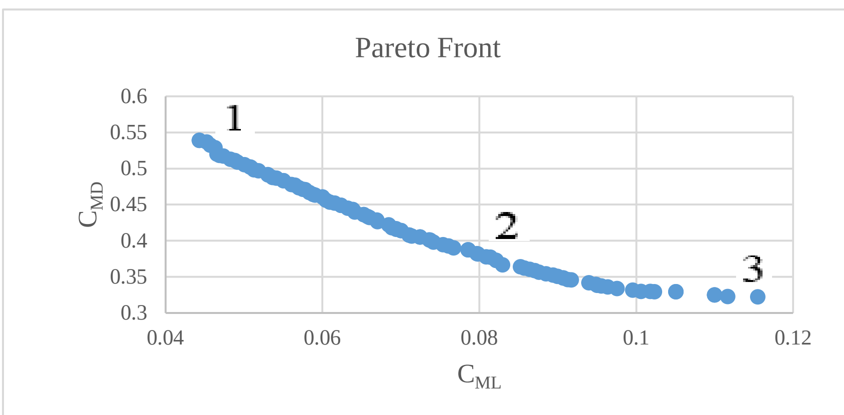


**Fig. 11.** Pareto-Front curve.

The efficiency of the proposed framework was investigated by optimizing the $C_{MD}$ and $C_{ML}$ in an optimization process based on the design variables $a_0$, $a_1$, $a_2$, $a_3$, $b_0$, $b_1$, and T. In the optimization process, the population size was considered to be 100, and crossover and mutation probabilities to be 0.6 and 0.1, respectively. After running the optimization for 500 generations, the optimization problem achieved convergence, and the PF curve was determined following the convergence (see Fig. 12). In the figure, the three optimal shapes were marked on PF, which are examined in the following parts of the present research.

The design variables and the objective functions of the three optimal shapes are presented in Table 1. As can be seen, the value of geometry parameter $b_1$ for the three optimal shapes is the same. Accordingly, the parameter $b_1$ significantly affects the amount of objective functions. The geometric parameter $b_1$ displays the curvature at the sides of the triangle. Therefore, all optimal shapes have the same curvature. This means that to minimize objective functions ($C_{MD}$ and $C_{ML}$) simultaneously, the design variable must be $b_1$=-28.443. The parameter TR as the cross-section size variations along the building height is the ratio of cross sectional area at the height H to the base of the building. TR for all optimal shapes varies from 0.4 to 0.5. The other design variables are close to zero indicating their low impact on objective functions. According to moment coefficient values (CML and CMD), sample1 and sample3 have the best performance in terms of lift and drag moment coefficients, respectively. The building shapes (plan and elevation) of the three samples are shown in Fig. 13.

**Table 1**. Design variables and the objective functions of three points on the Pareto Front curve.

| Design Variable | Sample1 | Sample2 | Sample3 |
|---|---|---|---|
| $a_0$ | 0.018 | 0.015 | 0.014 |
| $a_1$ | -0.016 | -0.014 | -0.021 |
| $a_2$ | 0.175 | 0.172 | 0.224 |
| $a_3$ | -0.518 | -0.529 | -0.607 |
| $b_0$ | 0.012 | 0.015 | 0.016 |
| $b_1$ | -28.443 | -28.443 | -28.443 |
| T(degree) | 168 | 149 | 121 |
| $C_{ML}$ | 0.044 | 0.091 | 0.116 |
| $C_{MD}$ | 0.539 | 0.348 | 0.322 |
| TR | 0.41 | 0.44 | 0.5 |

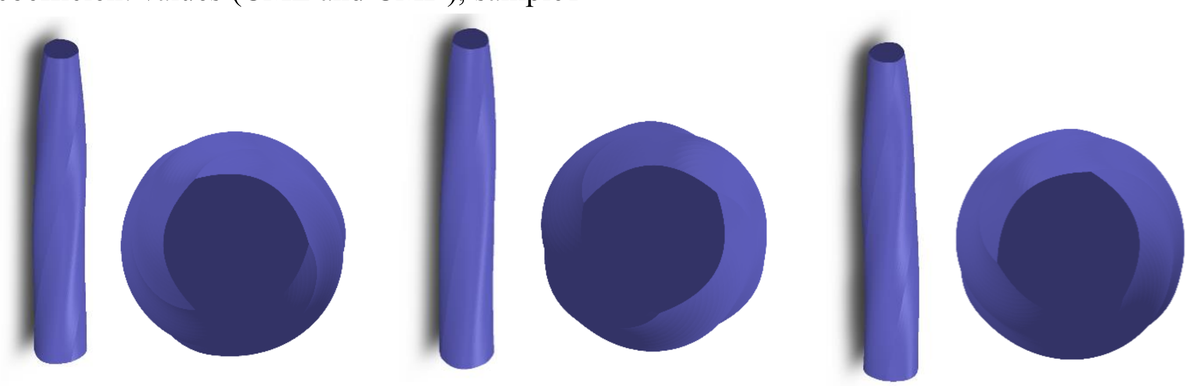

Sample 1 Sample2 Sample3

**Fig. 12.** The geometric shapes of buildings fitted on the Pareto Front curve (1, 2 and 3).

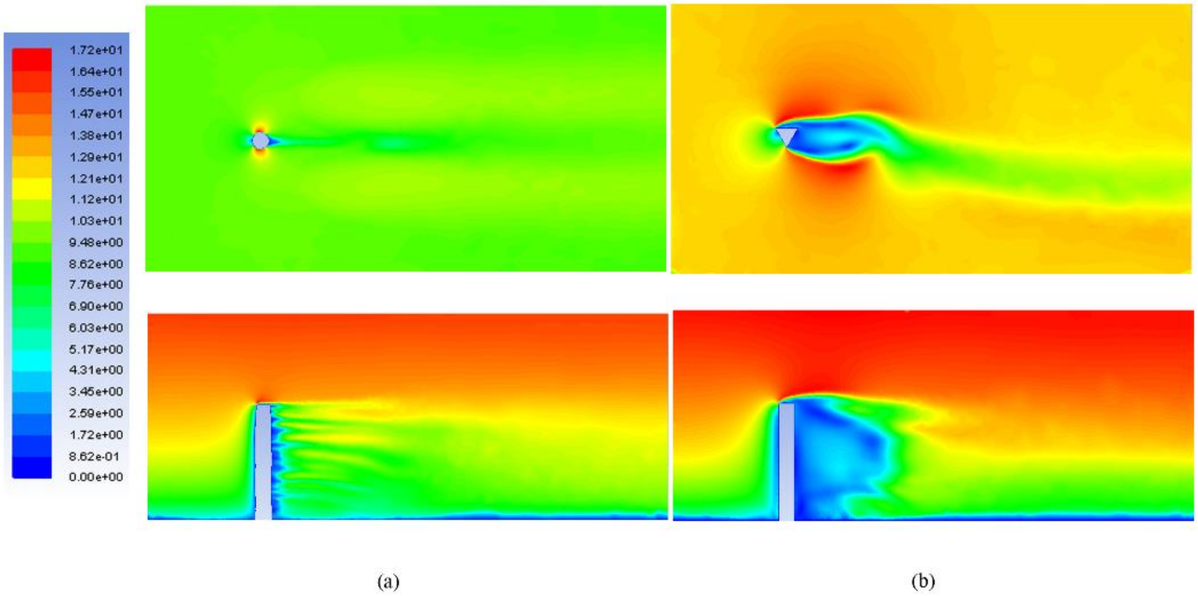

**Fig. 13.** Flow field around building at z=H/2: (a) optimal shape(Sample1) and (b) basic triangle shape.

Fig. 14 shows the mean velocity contour (m/s) of the wind flow for the sample 1 and the basic shape obtained from the CFD simulations. The flow pattern around the tall buildings was changed by means of the shape modifications, and the wake zone in the optimal shape was significantly smaller than the basic triangular shape. This shows that AOP plays an effective part in improving aerodynamic performance.

As can be seen in Fig. 15, the value of the twist angle, T, of the optimal shapes is in the range of $110^0$ to $170^0$. Also, $C_{MD}$ increases with increasing the twist angle and $C_{ML}$ decreases, which is due to changes in the flow pattern around the building.

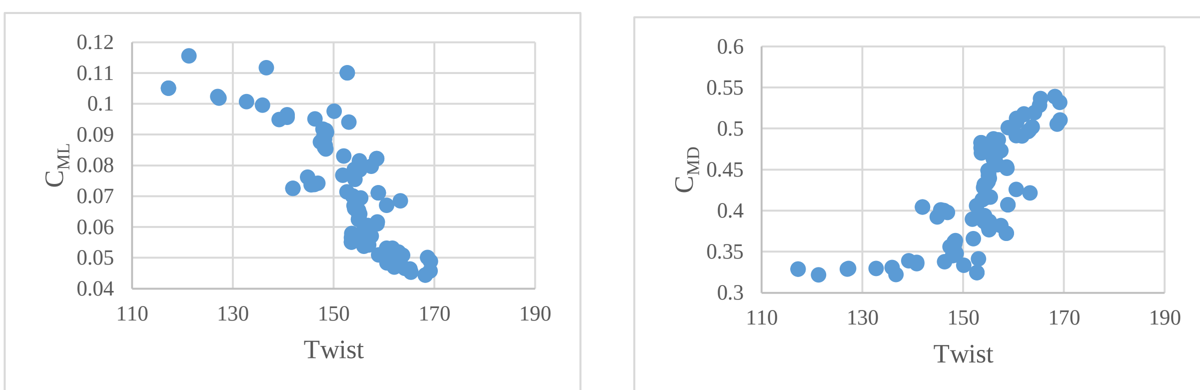


(a) (b)

**Fig. 14.** Diagram of the effect of twist angle variations on (a) $C_{ML}$ and (b) $C_{MD}$.

The mean moment coefficients $C_{MD}$ and $C_{ML}$ for the basic triangular building are 0.842 and 0.651, respectively. $C_{MD}$ and $C_{ML}$ of three optimal shapes, and ratios of these coefficients to the basic triangle shape are given in Table 2. The results show that for all optimal shapes, $C_{MD}$ is decreased by 36% to 62%, and $C_{ML}$ is reduced by 82% to 93%.

This indicates the significance of applying the aerodynamic modifications to mitigate aerodynamic responses.

**Table 2.** Comparison of Momentum Coefficients.

| Response | Sample1 | Sample2 | Sample3 |
|---|---|---|---|
| $C_{ML}$ | 0.044 | 0.091 | 0.116 |
| $C_{MD}$ | 0.539 | 0.348 | 0.322 |
| $C_{ML}$ ratio | 0.068 | 0.14 | 0.178 |
| $C_{MD}$ ratio | 0.64 | 0.413 | 0.382 |

## 7. Conclusions

The present research minimized the aerodynamic responses (mean moment coefficients) of tall buildings with trilateral cross-sections in an optimization process based on seven geometric variables. The geometrical parameters considered in the proposed strategy are capable of generating a wide range of external shapes of tall buildings with trilateral cross sections, and help to find the optimal aerodynamic shapes in an extensive search space.

An examination of the geometric parameters of the optimal shapes showed that the coefficient b1 for all the shapes laid on the PF has the same value b1=-28.443. This indicated the high impact of b1 parameter on the aerodynamic responses of the building. b1 Parameter defines the amount of the sides curvature hence, all optimal shapes obtained have fixed sides curvature.

Results showed that twist angle is another effective geometric parameter that directly related to the moment coefficient CMD, while inversely associated with the moment coefficient CML. The variations range of twist angle for optimal shapes obtained is $110^0$ to $170^0$. Also, other parameters due to their small effects are ignored.

In the proposed AOP process, $C_{MD}$ and $C_{ML}$ decreased by 62% and 93%, respectively. These results demonstrate that the AOP process can improve the aerodynamic performance of the trilateral tall buildings. Therefore, applying the AOP process before designing the building will significantly reduce construction costs.

## REFERENCES

[1] H. Hayashida and Y. Iwasa, “Aerodynamic shape effects of tall building for vortex induced vibration,” J. Wind Eng. Ind. Aerodyn., vol. 33, no. 1–2, pp. 237–242, Mar. 1990, doi: 10.1016/0167-6105(90)90039-F.

[2] S. Hajra and S. K. Dalui, “Numerical investigation of interference effect on octagonal plan shaped tall buildings,” Jordan J. Civ. Eng., vol. 10, no. 4, pp. 462–479, 2016.

[3] S. Mukherjee, S. Chakraborty, S. K. Dalui, and A. K. Ahuja, “Wind induced pressure on ‘Y’ plan shape tall building,” Wind Struct., vol. 19, no. 5, pp. 523–540, 2014, Accessed: Dec. 17, 2021. [Online]. Available: https://www.dbpia.co.kr/journal/articleDetail?nodeId=NODE10237151.

[4] T. Chen et al., “Study of flow characteristics in tunnels induced by canyon wind,” J. Wind Eng. Ind. Aerodyn., vol. 202, no. January, p. 104236, 2020, doi: 10.1016/j.jweia.2020.104236.

[5] K. C. S. Kwok and P. A. Bailey, "Aerodynamic Devices for Tall Buildings and Structures," J. Eng. Mech., vol. 113, no. 3, pp. 349–365, Mar. 1987, doi: 10.1061/(asce)0733-9399(1987)113:3(349).

[6] M. Gu and Y. Quan, "Across-wind loads of typical tall buildings," J. Wind Eng. Ind. Aerodyn., vol. 92, no. 13, pp. 1147–1165, Nov. 2004, doi: 10.1016/J.JWEIA.2004.06.004.

[7] L. Carassale, A. Freda, and M. Marrè-Brunenghi, "Experimental investigation on the aerodynamic behavior of square cylinders with rounded corners," J. Fluids Struct., vol. 44, pp. 195–204, 2014, doi: 10.1016/j.jfluidstructs.2013.10.010.

[8] K. P. You, Y. M. Kim, and N. H. Ko, "The evaluation of wind-induced vibration responses to a tapered tall building," Struct. Des. Tall Spec. Build., vol. 17, no. 3, pp. 655–667, Sep. 2008, doi: 10.1002/TAL.371.

[9] K. R. Cooper, M. Nakayama, Y. Sasaki, A. A. Fediw, S. Resende-Ide, and S. J. Zan, "Unsteady aerodynamic force measurements on a super-tall building with a tapered cross section," J. Wind Eng. Ind. Aerodyn., vol. 72, no. 1–3, pp. 199–212, Nov. 1997, doi: 10.1016/S0167-6105(97)00258-4.

[10] Y. M. Kim and K. P. You, "Dynamic responses of a tapered tall building to wind loads," J. Wind Eng. Ind. Aerodyn., vol. 90, no. 12–15, pp. 1771–1782, Dec. 2002, doi: 10.1016/S0167-6105(02)00286-6.

[11] Y. M. Kim, K. P. You, and N. H. Ko, "Across-wind responses of an aeroelastic tapered tall building," J. Wind Eng. Ind. Aerodyn., vol. 96, no. 8–9, pp. 1307–1319, Aug. 2008, doi: 10.1016/J.JWEIA.2008.02.038.

[12] Y. Kim and J. Kanda, "Characteristics of aerodynamic forces and pressures on square plan buildings with height variations," J. Wind Eng. Ind. Aerodyn., vol. 98, no. 8–9, pp. 449–465, Aug. 2010, doi: 10.1016/J.JWEIA.2010.02.004.

[13] Y. C. Kim and J. Kand, "Wind pressures on tapered and set-back tall buildings," J. Fluids Struct., vol. 39, pp. 306–321, May 2013, doi: 10.1016/J.JFLUIDSTRUCTS.2013.02.008.

[14] Y. C. Kim, J. Kanda, and Y. Tamura, "Wind-induced coupled motion of tall buildings with varying square plan with height," J. Wind Eng. Ind. Aerodyn., vol. 99, no. 5, pp. 638–650, May 2011, doi: 10.1016/J.JWEIA.2011.03.004.

[15] A. Sharma, H. Mittal, and A. Gairola, "Mitigation of wind load on tall buildings through aerodynamic modifications: Review," J. Build. Eng., vol. 18, pp. 180–194, Jul. 2018, doi: 10.1016/J.JOBE.2018.03.005.

[16] Y. C. Kim, E. K. Bandi, A. Yoshida, and Y. Tamura, "Response characteristics of super-tall buildings – Effects of number of sides and helical angle," J. Wind Eng. Ind. Aerodyn., vol. 145, pp. 252–262, Oct. 2015, doi: 10.1016/J.JWEIA.2015.07.001.

[17] B. E. Kumar, Y. Tamura, A. Yoshida, Y. C. Kim, and Q. Yang, "LOCAL AND TOTAL WIND FORCE CHARACTERISTICS OF

TRIANGULAR-SECTION TALL BUILDINGS," pp. 179–184, 2012.

[18] H. Tanaka, Y. Tamura, K. Ohtake, M. Nakai, and Y. Chul Kim, "Experimental investigation of aerodynamic forces and wind pressures acting on tall buildings with various unconventional configurations," J. Wind Eng. Ind. Aerodyn., vol. 107–108, pp. 179–191, Aug. 2012, doi: 10.1016/J.JWEIA.2012.04.014.

[19] Y. Tamura, Y. C. Kim, H. Tanaka, E. K. Bandi, A. Yoshida, and K. Ohtake, "Aerodyanmic and response characteristics of super-tall buildings with various configurations," Proc. 8th Asia-Pacific Conf. Wind Eng. APCWE 2013, pp. K219–K243, 2013, doi: 10.3850/978-981-07-8012-8_Key-12.

[20] A. Kareem, S. M. J. Spence, E. Bernardini, S. Bobby, and D. Wei, "Using computational fluid dynamics to optimize tall building design," CTBUH J., no. 3, pp. 38–43, 2013.

[21] E. Bernardini, S. M. J. Spence, D. Wei, and A. Kareem, "Aerodynamic shape optimization of civil structures: A CFD-enabled Kriging-based approach," J. Wind Eng. Ind. Aerodyn., vol. 144, pp. 154–164, Sep. 2015, doi: 10.1016/J.JWEIA.2015.03.011.

[22] A. Elshaer, G. Bitsuamlak, and A. El Damatty, "Enhancing wind performance of tall buildings using corner aerodynamic optimization," Eng. Struct., vol. 136, pp. 133–148, Apr. 2017, doi: 10.1016/J.ENGSTRUCT.2017.01.019.

[23] A. Elshaer and G. Bitsuamlak, "Multiobjective Aerodynamic Optimization of Tall Building Openings for Wind-Induced Load Reduction," J. Struct. Eng., vol. 144, no. 10, p. 04018198, Aug. 2018, doi: 10.1061/(ASCE)ST.1943-541X.0002199.

[24] M. Noormohamadian and E. Salajegheh, "Evaluation and minimization of moment coefficient of tall buildings with trilateral cross-section via a surrogate model," SN Appl. Sci., vol. 3, no. 2, pp. 1–14, Feb. 2021, doi: 10.1007/S42452-020-04128-5/FIGURES/14.

[25] "SolidWorks 2016 Reference Guide: A comprehensive reference guide with over ... - David Planchard - Google Books." https://books.google.com/books?hl=en&lr=&id=5VgACwAAQBAJ&oi=fnd&pg=PP3&dq=D.+Planchard,+SolidWorks+2015+Refrence+Guide,+Sdc+Publications.&ots=FZbqb9AanV&sig=VcI3JNw8zRnq3anznxJ2YmFBZCg#v=onepage&q=D. Planchard%2C SolidWorks 2015 Refrence Guide%2C Sdc Publications.&f=false (accessed Dec. 17, 2021).

[26] T. D. Canonsburg, "ANSYS Fluent Tutorial Guide," vol. 15317, no. November, pp. 724–746, 2013.

[27] Y. Tominaga et al., "AIJ guidelines for practical applications of CFD to pedestrian wind environment around buildings," J. Wind Eng. Ind. Aerodyn., vol. 96, no. 10–11, pp. 1749–1761, 2008, doi: 10.1016/j.jweia.2008.02.058.

[28] Q. Li, J. Fang, A. Jeary, and D. Paterson, "Computation of wind loading on buildings by CFD," Hong Kong Institution of Engineers, Transactions, 1998.

https://scholar.google.com/scholar?hl=en&as_sdt=0%2C5&q=Computation+of+Wind+Loading+on+Buildings+by+CFD&btnG= (accessed Dec. 17, 2021).

[29] LAUNDER and B. E., “Modeling flow-induced oscillations in turbulent flow around a square cylinder,” ASME Fluid Eng. Conf. 1993, 1993, Accessed: Dec. 17, 2021. [Online]. Available: https://ci.nii.ac.jp/naid/80007747037.

[30] M. Yahyai, A. S. Daryan, S. M. Mirtaheri, and M. Ziaei, “Wind Effect on Milad Tower Using Computational,” 2009.

[31] S. Huang, Q. S. Li, and S. Xu, “Numerical evaluation of wind effects on a tall steel building by CFD,” J. Constr. Steel Res., vol. 63, no. 5, pp. 612–627, May 2007, doi: 10.1016/J.JCSR.2006.06.033.

[32] “Goldberg, D. (1989). “Genetic Algorithms in Search.... - Google Scholar.” https://scholar.google.com/scholar?hl=en&as_sdt=0%2C5&q=Goldberg%2C+D.+%281989%29.+“Genetic+Algorithms+in+Search.+Optimization+and+Machine+Learning.&btnG= (accessed Dec. 17, 2021).

[33] “Davis, L. (1991). Handbook of Genetic Algorithms,... - Google Scholar.” https://scholar.google.com/scholar?hl=en&as_sdt=0%2C5&q=Davis%2C+L.+%281991%29.+Handbook+of+Genetic+Algorithms%2C+Van+Nostrand+Reinhold&btnG= (accessed Dec. 17, 2021).

[34] K. Deb, A. Pratap, S. Agarwal, and T. Meyarivan, “A fast and elitist multiobjective genetic algorithm: NSGA-II,” IEEE Trans. Evol. Comput., vol. 6, no. 2, pp. 182–197, Apr. 2002, doi: 10.1109/4235.996017.

[35] S. Jung, J. Ghaboussi, and S.-D. Kwon, “Estimation of Aeroelastic Parameters of Bridge Decks Using Neural Networks,” J. Eng. Mech., vol. 130, no. 11, pp. 1356–1364, Nov. 2004, doi: 10.1061/(ASCE)0733-9399(2004)130:11(1356).

[36] T. Wu and A. Kareem, “Modeling hysteretic nonlinear behavior of bridge aerodynamics via cellular automata nested neural network,” J. Wind Eng. Ind. Aerodyn., vol. 99, no. 4, pp. 378–388, Apr. 2011, doi: 10.1016/J.JWEIA.2010.12.011.

[37] C. Lee, J. Kim, D. Babcock, and R. Goodman, “Application of neural networks to turbulence control for drag reduction,” Phys. Fluids, vol. 9, no. 6, p. 1740, Jun. 1998, doi: 10.1063/1.869290.

[38] P. Wasserman, “Advanced methods in neural computing,” 1993, Accessed: Dec. 17, 2021. [Online]. Available: https://dl.acm.org/doi/abs/10.5555/562821.

[39] K. Hornik, M. Stinchcombe, and H. White, “Multilayer feedforward networks are universal approximators,” Neural Networks, vol. 2, no. 5, pp. 359–366, Jan. 1989, doi: 10.1016/0893-6080(89)90020-8.